Appl. Phys. A 37, 95–108 (1985)

Applied Physics A Solids and Surfaces

© Springer-Verlag 1985

Computer Simulation of Two-Component Target Sputtering

W. Eckstein

Max-Planck-Institut für Plasmaphysik, EURATOM Association, D-8046 Garching bei München, Fed. Rep. Germany

J. P. Biersack

Hahn-Meitner-Institut für Kernforschung, D-1000 Berlin 39

Received 28 August 1984/Accepted 29 January 1985

Abstract. The TRIM SP computer simulation program, which is based on the binary collision approximation, is applied to sputtering of two component targets. The topics discussed in this paper are: contribution of different processes leading to sputtering, total and partial sputtering yields, surface compositions at stationary conditions, sputtering of isotopic mixtures, angular and energy distributions and the escape depth of sputtered particles. Targets investigated are TaC, WC, TiC, TiD_2, and B (as an isotope mixture), bombarded by the noble gas ions and D (in the case of TiD_2). Comparison with experimental data and calculated results show good agreement demonstrating that collisional effects are sufficient to describe the experimental data in the examples investigated.

PACS: 79.20

The sputtering of monoatomic targets is quite well understood due to the many experimental and theoretical investigations described in the compilation edited by Behrisch [1]. We have shown that Monte Carlo calculations [2] are quite effective for a better understanding of sputtering as well as reproducing experimental data quantitatively. This success stimulated the wish to investigate the sputtering of two-or multicomponent targets. The first step is a program, which takes more than one component into account but does not store the composition changes due to the bombardment fluence. The second step is to dynamically rearrange the target composition during sputtering. This last point is a further refinement, which has previously been published [3, 4]. In this paper we will restrict ourselves to the static program handling a compound target of only two components for the reason of clarity and simplicity. It is clear that this static program can be used mainly for sputtering at low fluences where the stoichiometric changes in the target remain small. But it allows investigations of partial sputtering yields, energy and angular distributions and possible differences in these results for the two components. Comparison with results from elementary targets are also possible and the dependence of incident ion energy and angles is studied. Mass and bonding effects are investigated by choosing suitable targets. Furthermore it seems possible to use the static program to calculate equilibrium surface compositions by changing the composition until the sputtered atom flux reflects the stoichiometric bulk composition. The use of the TRIM sputtering program implies that only randomized (amorphous) targets are studied; spike effects, diffusion, segregation, recoil implantation and cascade mixing are not included. Comparison with experimental data is performed as far as possible. For further information on multicomponent sputtering the recent reviews by Betz and Wehner [5], and by Andersen [6] are recommended. An approach to study the sputtering of compound targets by an analytical theory is given in [7–9].

The calculated data are of interest not only in fundamental aspects of sputtering, but also in any kind of analysis by ion bombardment as, for example, in SIMS

[10]. Some examples investigated as the carbides are of importance in plasma-wall interaction [11, 12].

1. The Monte Carlo Program

The TRIM Monte Carlo program, version TRSP2C, used in this paper is an extension of the sputtering TRIM version TRSP1C described in [2]. To study the main effects of sputtering of compound targets, we have limited the number of target constituents to two. This static program is mainly valid for low ion fluences (virgin sample), so that also the implanted species can be neglected. The composition of the target is given by the input data and the collision partner is chosen randomly proportional to its fraction in the target composition. The surface binding energies for the two target species can be chosen independently. For the inelastic energy loss Bragg's rule (linear interpolation due to the composition) is applied. These are the only changes introduced in the monoatomic target program. It should be remembered, that the sputtering TRIM program is based on the binary collision model and the target has a randomized structure.

For the choice of the surface binding energies two ways have been applied:

1) Each target species has the same surface binding energy which is determined by the heat of atomization

$$\Delta H_{at} = 2\Delta H_f(AB) + \Delta H_s(A) + \Delta H_s(B)\,, \tag{1}$$

where ΔH_s is the heat of sublimation and ΔH_f is the heat of formation of the molecule. The surface binding energy of the components A and B is

$$E_s^c(A) = E_s^c(B) = \Delta H_{at}/n\,, \tag{2}$$

where n is the number of atoms in the molecule.

2) For the study of equilibrium surface composition we choose for a compound AB and for the depleted species B

$$E_s^c(B) = \Delta H_s(B) + \Delta H_f(AB) \tag{3}$$

because atom B will always come from the molecule AB. For the surface enriched component A the choice is a linear interpolation between

$$E_s^c(A) = \Delta H_s(A) + \Delta H_f(AB) \tag{4}$$

and $\Delta H_s(A)$ due to the composition, because atoms A will orginate partly from the molecule and partly from pure material A.

The results shown in the next sections do not depend on the choice of the surface binding model as long as the heat of formation is small in comparison to the heat of sublimation.

Before discussing the results it should be kept in mind as shown in this chapter that the program treats only collisional effects as in the analytical theory. That means any effects as thermal or radiation-enhanced diffusion and segregation are not taken into account. Also collisional mixing and recoil implantation are neglected (but they were discussed in [4, 13]). If these effects play an important role, the calculated results are not expected to agree with experimental data. But the calculated data give the pure collisional effects and comparing the calculated data with experimental results may give an idea about the contribution of the non-collisional effects mentioned above. The calculations described here are valid only for starting conditions or low bombardment doses. The justification for calculations at equilibrium conditions is given in Sect. 2.2.

2. Results

2.1. Processes Contributing to Sputtering

As shown in [2] we distinguish four processes which lead to sputtering of a target atom. A sputtered particle can be a primary knock-on atom (PKA), which was hit by an incident ion, or it can be a secondary knock-on atom (SKA), which was set in motion by another target atom. The second distinction is the direction of the incident ion, which lead to the sputtered particles: The incident ion can move into the solid (Ion in) or it may be moving toward the surface (Ion out). The distinction is made by the sign of the cosine with respect to the surface normal. Three examples have been chosen, the bombardment of TaC by Ne in Fig. 1, and the bombardment of WC by ^{4}He and Xe at normal incidence in Figs. 2 and 3. The contributions of the four processes to the sputtering of Ta(W) and C versus the energy of the incident ion are shown. In addition the figures exhibit the partial sputtering yields. For Ta the process (Ion out, PKA) is the dominant one below 1 keV, whereas the process (Ion in, PKA) is only a small contribution over the whole energy range investigated. For C both PKA-processes are important. The overall trend of the contributions of the four different processes are similar to those in monoatomic targets [2] for C, however, the process (Ion in, PKA) is stronger in TaC than in C and the (Ion out) process are negligible small in C. The partial yields shown at top in Figs. 1 and 2 show large differences in the absolute values as well as in the energy of maximum yield. The differences in yield will lead to an enrichment of Ta at the surface. A measure of this Ta enrichment is demonstrated by the relative carbon yield also given in the Figs. 1 and 2. The ratio of the carbon yield $Y(C)$ to the total yield $Y = Y(C) + Y(Ta)$ becomes 0.5 for stoichiometric sputtering; this ratio becomes 1 if the sputtering threshold for the heavier component is reached.

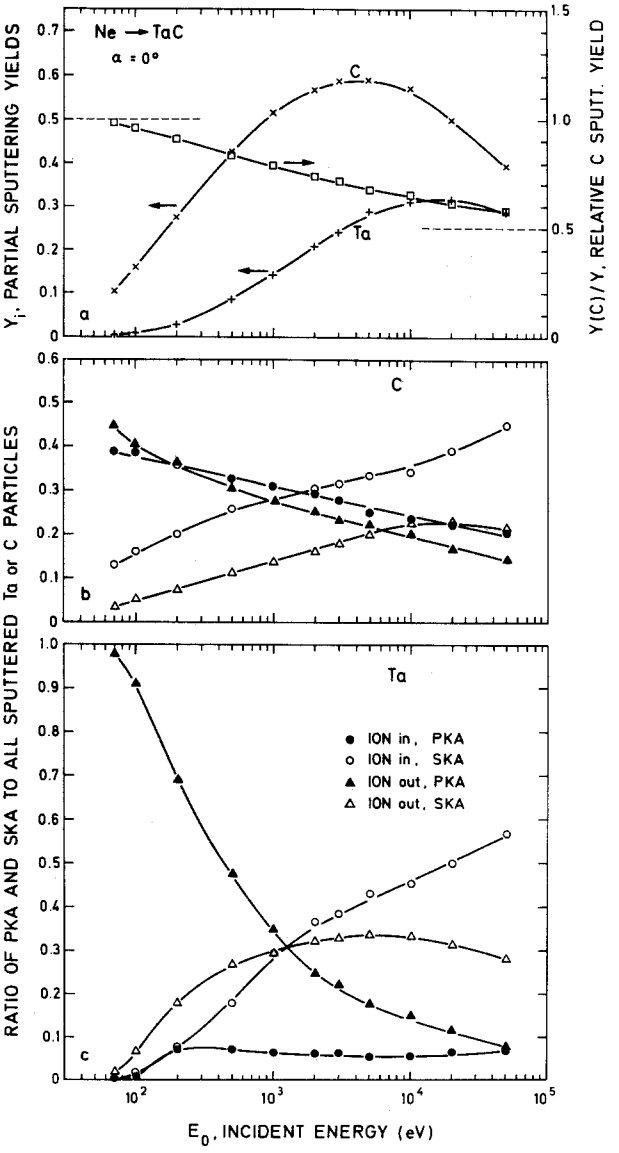

Fig. 1a–c. Ne bombardment of TaC at normal incidence, $\alpha = 0°$. (a) Partial sputtering yields, Y(Ta) and Y(C), and the relative partial yield of C, $Y(C)/[Y(C)+Y(Ta)]$, versus the incident energy, E_0. (b) and (c) Relative contributions of primary knock-on atoms, PKA (Ion in and Ion out), and secondary knock-on atoms, SKA (Ion in and Ion out), to the partial sputtering yields for C (b) and Ta (c). Lines drawn to guide the eye

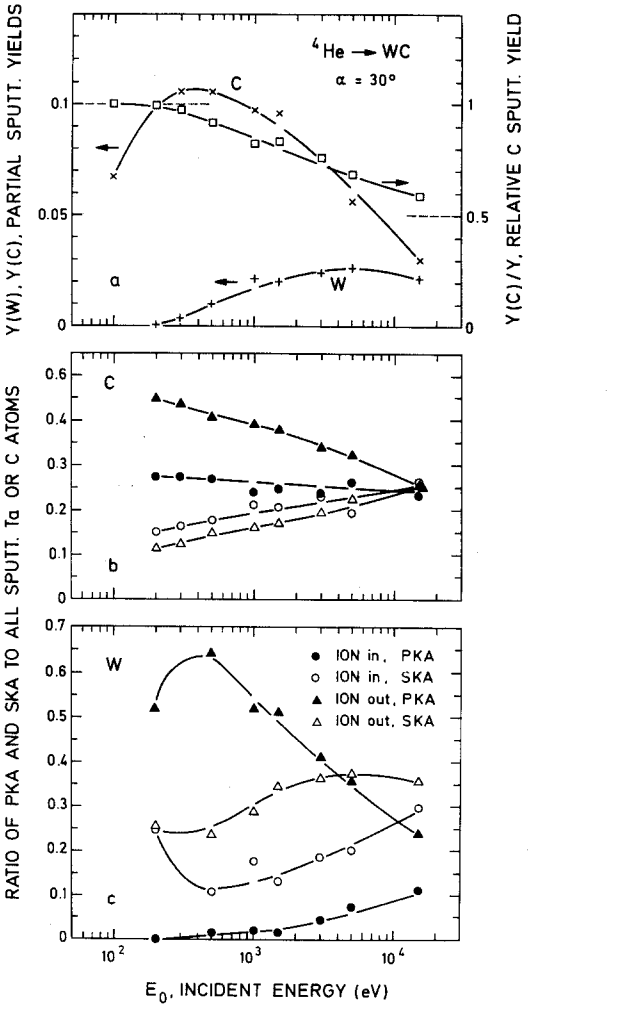

Fig. 2. ^{4}He bombardment of WC at an angle of incidence, $\alpha = 30°$. Description the same as for Fig. 1

In Fig. 3 it is demonstrated for the bombardment of WC by Xe, that for both species W and C the processes (Ion in, PKA) and (Ion in, SKA) dominate. The partial yields have a similar energy dependence. An appreciable enrichment of W at the surface will build up at energies below 0.15 keV.

For the bombardment of TaC with 1 keV Ne the contribution of the four processes versus the angle of incidence is shown in Fig. 4. The dependence of the contributions on the angle of incidence, measured from the target surface normal, is stronger for Ta than for C. The main feature is the increasing contribution of the process (Ion in, PKA) with increasing angle of incidence. The partial yields show a similar behaviour with the angle of incidence. The relative carbon yield exhibits only a small dependence on the angle of incidence, demonstrating that the Ta enrichment is only weakly dependent on the angle of incidence.

2.2. *Surface Concentrations*

The idea to calculate surface concentrations with the static program is the following: The surface concentration has to be changed so that the partial sputtering yields are equal. The concentration in the bulk is depth dependent from the surface to some depth with the bulk value. The depth range of this concentration profile is dependent on the ion-target combination and the incident ion energy. But nearly all

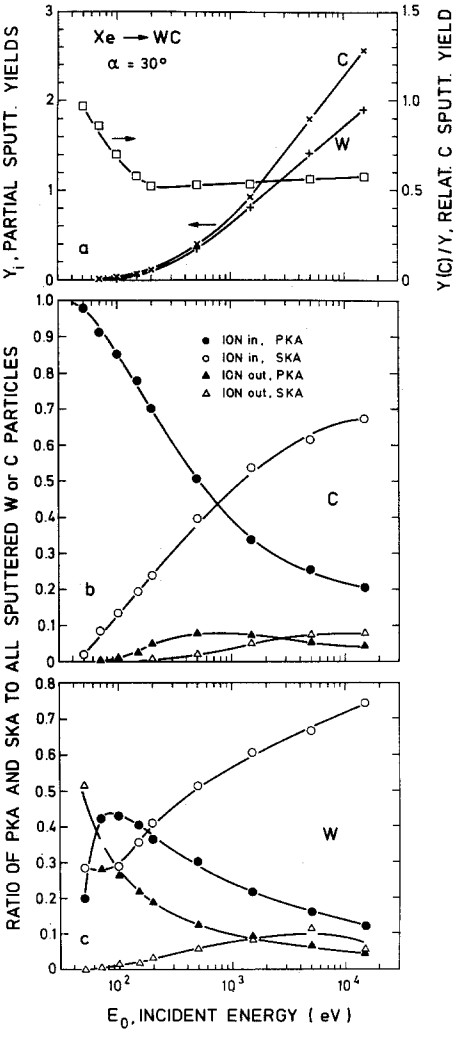

Fig. 3. Xe bombardment of WC at an angle of incidence, $\alpha = 30°$. Description the same as for Fig. 1

sputtered particles originate from the first two atomic layers, in which no drastic comcentration changes will happen. The calculations are restricted to the low energy range, where the contributions of PKA are important (Figs. 1–4). This means only a very shallow depth is important for sputtering. Therefore we changed the target composition and correspondingly the density and the surface binding energies, as indicated in Sect. 1 until the sputtered flux of atoms reflects the stoichiometric bulk composition. This is certainly an approximation, but it proved to be in good agreement with results from the dynamic program [13], and it has the advantage of consuming less computing time. The choice of targets was WC, TaC, and TiC, because for these three targets experimental data exist [14, 15]. WC and TaC are chosen because the preferential sputtering or surface enrichment is mainly a mass effect, as the binding energies of the constituents are similar and much larger than the heat of formation of the molecules (1–4) [16]. In the case of TiC there is still a mass effect, but the species with the lower mass, C, has a higher surface binding energy than Ti, so that for the lighter ion the mass effect should be partly cancelled by a bonding effect. Figure 5 demonstrates the determination of the surface equilibrium concentration. The relative W sputtering yield and the partial yields are plotted versus the composition x. The value x_{eq}, where the relative yield is 0.5 or the partial yields are equal, gives the surface equilibrium concentration. x is not varied below 0.5, because there is clearly a W enrichment. The surface equilibrium concentrations for WC and TiC are plotted for the bombardment with different incident ions versus the energy of the incident ion in Fig. 6. The angle of incidence, $\alpha = 30°$, is chosen to meet the experimental conditions [14, 15]. The experiments usually exhibit a lower surface enrichment than the calculations, but the overall agreement with the experimental results is reasonable, especially the energy dependence. In the experiments it is assumed that for 1 keV Xe bombardment the preferential sputtering is negligible. By taking the calculated enrichment for Xe bombardment into account one would obtain better agreement for the light ions. The lower enrichments found in experiments may also be due to surface roughness and due to the Auger technique which averages over more than 10 Å depth. The higher experimental Ti enrichment for hydrogen bombardment may have to do with chemical effects [17]. It should be noticed that also for Xe, where the energy transfer to W is more effective than to C, a W enrichment at the surface builds up. The differences between WC and TiC are partly due to bonding effects.

The calculated results indicate that collisional effects are sufficient to explain the experimental findings. In the examples studied any kind of diffusion and segregation are not important. Also collisional mixing seems to be negligible because of the nearly identical results from the procedure used here and in the dynamic program [18].

In Fig. 7 it is demonstrated that the surface equilibrium concentration is only weakly dependent on the angle of incidence.

2.3. Total Yields

Total yields (and partial yields) cannot be compared in most cases, because the calculation gives only the starting conditions, whereas experimentally the yields are determined after bombardment of a large dose to measure the weight loss of the target. The only way to make a reasonable comparison is to use the same method as in the last subsection to calculate the yields

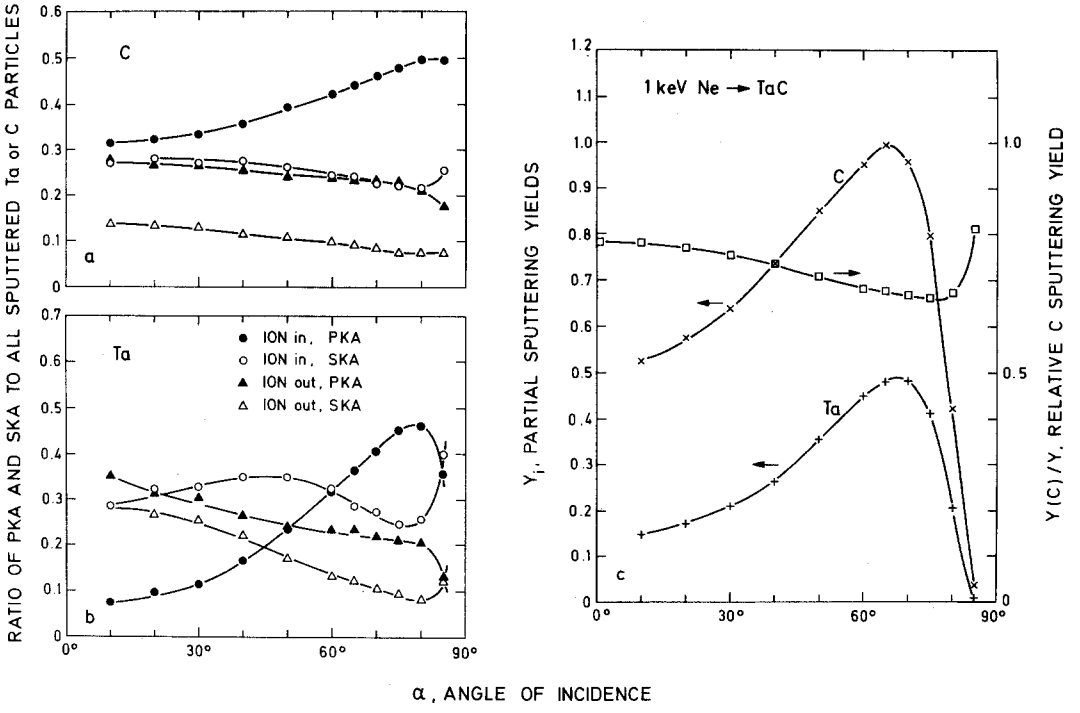

Fig. 4a–c. Ne bombardment of TaC at an incident energy, $E_0 = 1$ keV. (c) Partial sputtering yields, Y(Ta) and Y(C), and the relative partial yield of C, $Y(C)/Y$, versus the angle of incidence α. (a) and (b) Description as in Fig. 1

for a composition, where stoichiometric sputtering occurs. The results of such a calculation is shown in Fig. 8 for the bombardment of WC by ^{4}He at an incident angle, $\alpha = 30°$. The total yield at starting conditions ($x = 0.5$) is much larger at energies below 1 keV than the yields at equilibrium ($x > 0.5$). For increasing W concentration the yield decreases with decreasing energy, because of the small energy transfer from ^{4}He to W. At low energies the yield from WC

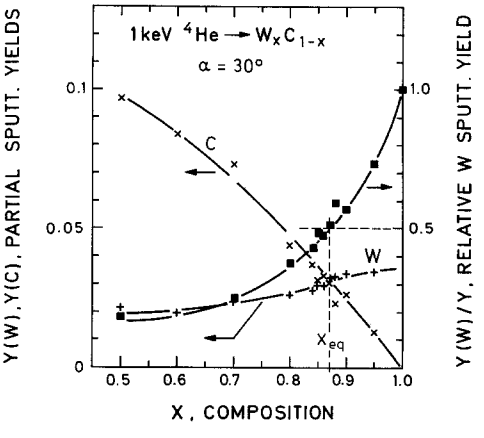

Fig. 5. Partial sputtering yields, Y(W) and Y(C), and relative partial sputtering yield, $Y(W)/Y[Y = Y(W) + Y(C)]$, versus the composition x. W_xC_{1-x} was bombarded by 1 keV ^{4}He at an incident angle, $\alpha = 30°$

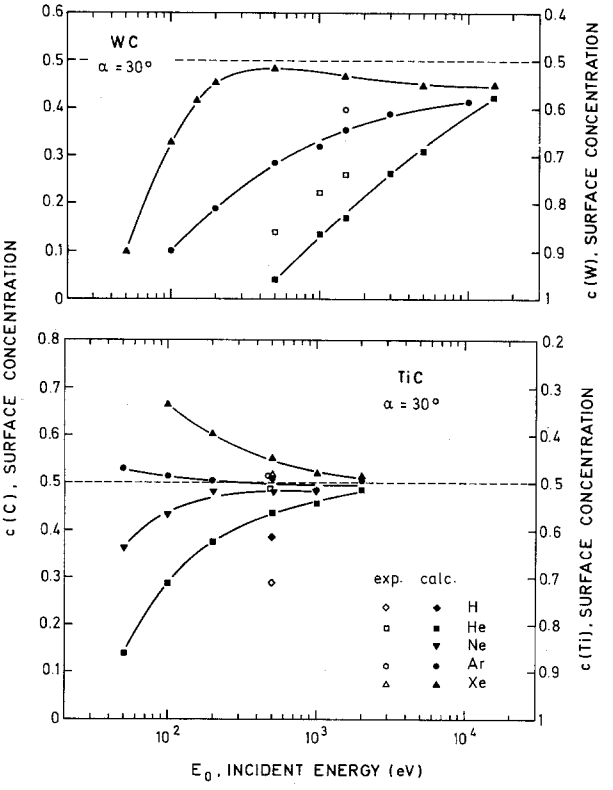

Fig. 6. Surface concentrations at stationary conditions (stoichiometric sputtering) versus the incident energy, E_0. WC and TiC are bombarded by H, ^{4}He, Ne, Ar, and Xe at an incident angle, $\alpha = 30°$. Experimental data from [14, 15]

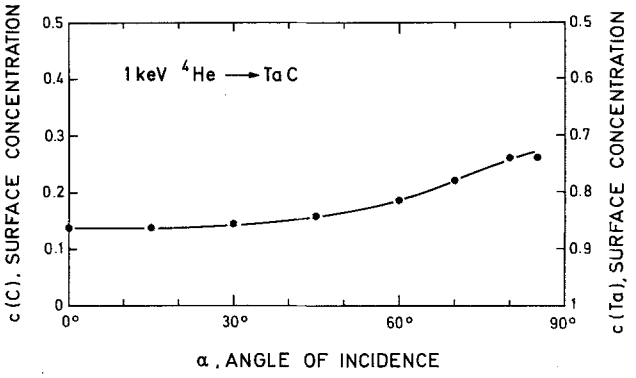

Fig. 7. Surface concentrations at stationary conditions (stoichiometric sputtering) versus the angle of incidence α. TaC is bombarded by 1 keV ^{4}He

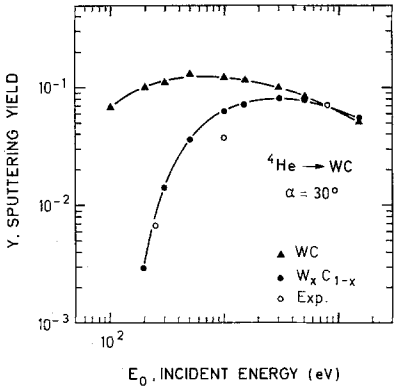

Fig. 8. Total yields for nominal composition, WC, and for stationary conditions, W_xC_{1-x}, versus the incident energy E_0. Bombardment with ^{4}He at an incident angle, $\alpha=30°$. Comparison with experimental data [19]

should approach that of W. The experimental data [19] show the same energy dependence as the calculated ones, the agreement on an absolute scale is within a factor of 2. The experiments were performed at normal incidence, where the yields are slightly lower than those at an angle of incidence, $\alpha=30°$. Total and partial sputtering yields of borides and other carbides have been investigated experimentally [19, 20] and by a TRIM SP computer simulation [21].

2.4. *Sputtering of Isotopic Mixtures*

The sputtering of elements, which consist of different isotopes is an example of a compound (or homogeneous alloy), where both species have the same surface binding energy but a different mass although the mass difference is small. The largest effect can be expected for an isotopic mixture, where the relative mass difference is large. This was the reason to choose boron (80% ^{11}B, 20% ^{10}B assumed natural isotope composition),

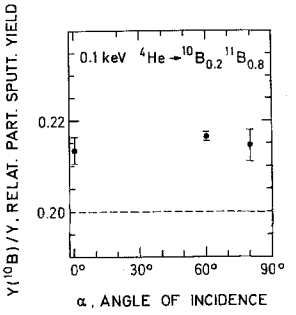

Fig. 9. Relative partial sputtering yield of ^{10}B versus the angle of incidence α. $^{10}B_{0.2}$ $^{11}B_{0.8}$ is bombarded by 0.1 keV ^{4}He

where the relative mass difference is about 10%. As shown in Fig. 9, the relative partial sputtering yield $[Y(^{10}B)/(Y(^{10}B)+Y(^{11}B)]$ is nearly independent of the angle of incidence as was also demonstrated in Sect. 2.2. The figure shows that in this case of the bombardment of boron with 0.1 keV helium the difference of the partial yield of ^{10}B is about 8% larger than expected from the isotope ratio. This leads to an enrichment of ^{11}B at the surface. The small dependence of the relative yields on the angle of incidence is the reason to choose for all isotope sputtering calculations an angle of incidence, $\alpha=60°$, because at this incident angle the yields are higher. This leads to better statistics or needs shorter computing times. The dependence of the relative partial yields on the incident ion at a fixed ion energy of 1 keV is small for heavier incident ions but increases for the light ions as shown in Fig. 10. However, at 0.1 keV ^{4}He produces an enrichment of ^{11}B, whereas with increasing incident mass the situation is changing to an enrichment of ^{10}B for the bombarding with Xe. The energy dependence of the relative partial yield for He and Xe as incident ions are shown in Fig. 11. As one would expect from the energy transfer in a binary collision He sputters more efficiently the lighter isotope ^{10}B, whereas Xe yields a higher sputtering for the heavier isotope ^{11}B at least at

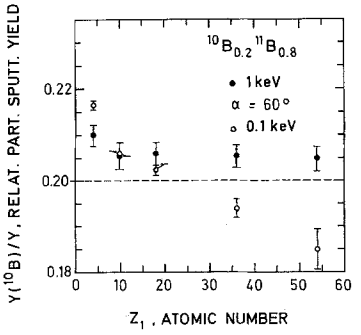

Fig. 10. Relative partial sputtering yield of ^{10}B versus the nuclear charge Z_1 of the incident particles. $^{10}B_{0.2}$ $^{11}B_{0.8}$ is bombarded at 1 and 0.1 keV at an incident angle, $\alpha=60°$

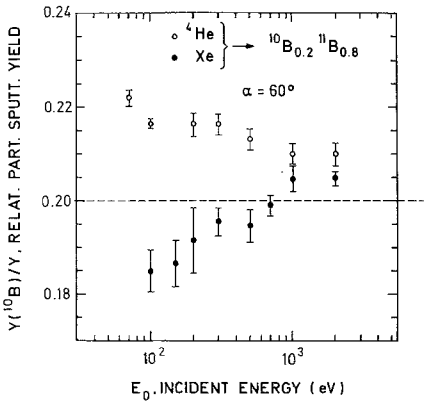

Fig. 11. Relative partial sputtering yield of ^{10}B versus the incident energy, E_0. $^{10}B_{0.2}$ $^{11}B_{0.8}$ is bombarded by ^4He and Xe at an incident angle, $\alpha = 60°$

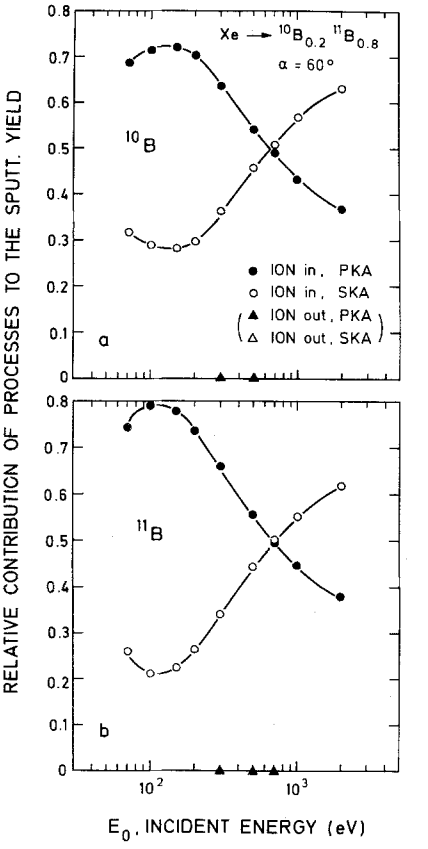

Fig. 12a and b. Relative contributions of different processes (Ion in, PKA and SKA) to the partial yields of (a) ^{10}B, (b) ^{11}B by Xe bombardment of $^{10}B_{0.2}$ $^{11}B_{0.8}$ at an incident angle, $\alpha = 60°$. The contribution of processes (Ion out, PKA and SKA) are negligibly small

low energies. But for Xe the relative ^{10}B yield increases with increasing energy yielding no preferential sputtering at about 700 eV and a higher sputtering of the light isotope above 1 keV. This may be explained by the processes which lead to sputtering: the process (Ion in, PKA) is dominant below 0.7 keV, the process (Ion in,

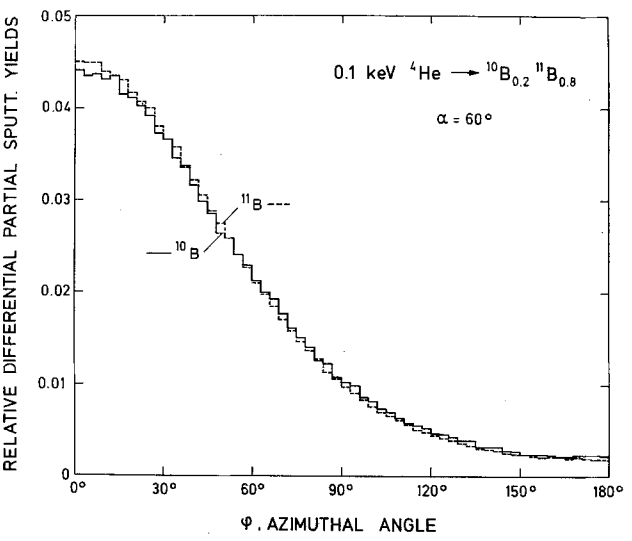

Fig. 13. Relative differential partial sputtering yields of ^{10}B and ^{11}B versus the azimuthal angle φ (integrated over the energy E and the polar angle β). $^{10}B_{0.2}$ $^{11}B_{0.8}$ is bombarded by 0.1 keV ^4He at an angle of incidence, $\alpha = 60°$

SKA) takes over above 0.7 keV (Fig. 12), i.e. at higher incident energies the sputtering is a result of cascade formation, which involves both isotopes independent of the PKA. It also justifies the consideration in [22], that the processes (Ion in, PKA, SKA) are the dominant ones.

[Ref. 8, Eq. (11b)] derived from the analytical theory yields a relative yield difference, $\delta = 0.0323$ assuming a power potential exponent $m = 1/6$ [2]. The corresponding value determined from the relative yield of 2 keV Xe bombardment (where the analytical theory should be applicable) in Fig. 11 is $\delta = 0.0314$. It is interesting to note that from experimental sputtering data of isotropic mixtures a value $m \approx 0.2$ was derived [6].

Sputtering by 0.1 keV ^4He at an incident angle, $\alpha = 60°$, as shown in Figs. 13 and 14, demonstrates clearly that the lighter component ^{10}B is preferentially emitted in the backward direction and into smaller polar angles, which is in agreement with earlier experimental results by Wehner et al. [23] for U. The differences are of the order of 2% and experimental investigations of D bombardment of B were not sensitive enough to see this effect [24].

For the heavier isotopic targets, e.g. Cu, for example preferential sputtering is a percent effect and it needs long computing times to ensure a quantitative result.

2.5. *Angular Distributions*

The angular distributions of sputtered Ta and C for normal incidence are shown in Fig. 15. The C distributions exhibit for all conditions investigated an

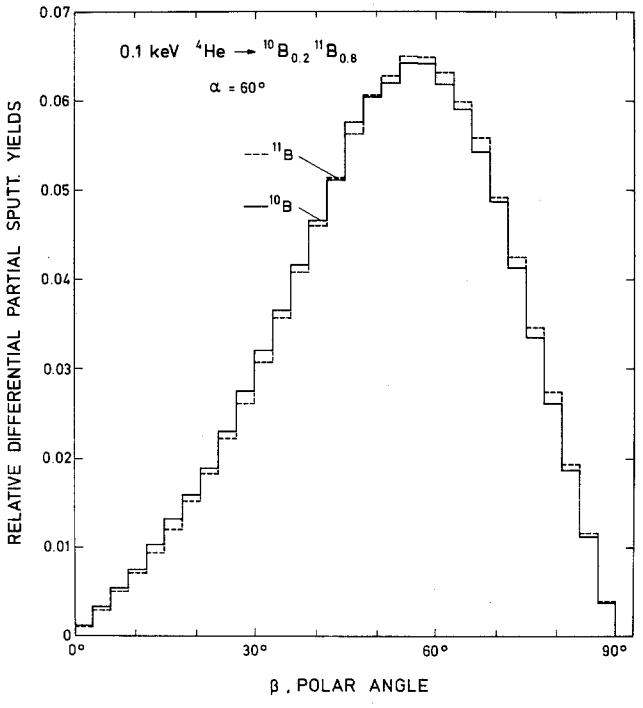

Fig. 14. Relative differential partial sputtering yields of ^{10}B and ^{11}B versus the polar angle β (integrated over the energy E and the azimuthal angle φ). $^{10}B_{0.2}$ $^{11}B_{0.8}$ is bombarded by 0.1 keV ^{4}He at an angle of incidence, $\alpha = 60°$

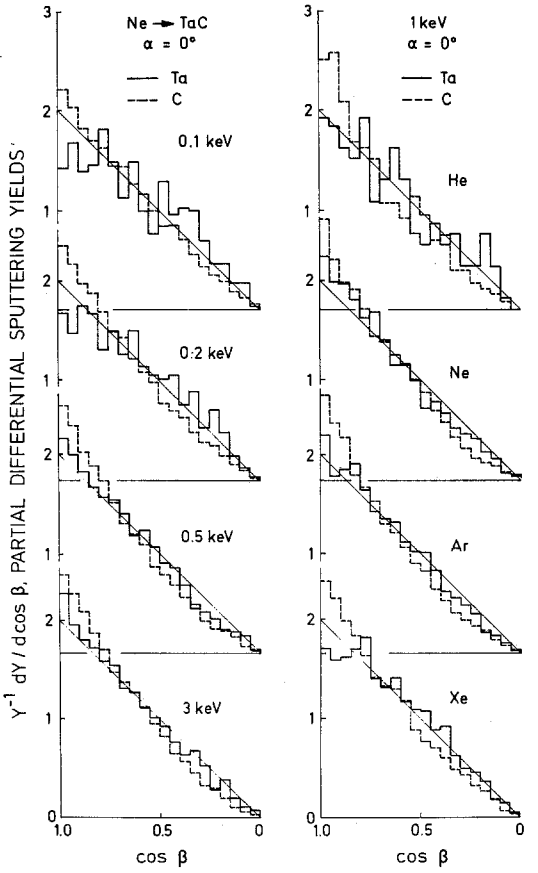

Fig. 15a and b. The differential partial sputtering yields of sputtered Ta and C atoms versus the cosine of the polar emission angle β for normal incidence, $\alpha = 0°$. The straight line indicates a cosine distribution. (a) Ne bombardment of TaC at 4 incident energies E_0; (b) bombardment of TaC with 1 keV ^{4}He, Ne, Ar, and Xe

overcosine distribution, whereas the Ta distributions are undercosine for low energies and for heavy incident particles. With increasing energy also the Ta distributions become overcosine which is the same behaviour as for monoatomic targets [2].

For non-normal incidence the sputtered particles have a strong forward directed emission, which is shown for two targets TaC and TiC but for the same incident conditions in Fig. 16. The azimuthal angular distribution (integrated over all polar angles) is shown here. The Ta and Ti distributions are quite different, the Ta distribution is more forward peaked. Also the two C distributions are not equal, the C distribution for the bombardment of TaC has a larger backward contribution than for TiC due to the enhanced probability of backscattering of He and C from Ta than from Ti. Angular distributions (for non-normal incidence) in the incident plane (defined by the target normal and the incident beam), by which we mean an intensity in an azimuthal angular range $0° < |\varphi| < 15°$ and $165° < |\varphi| < 180°$, are shown in the next Figs. 17 and 18. In Fig. 17 it is demonstrated that the C and the Ti distributions have a strongly peaked distribution, whereas the Ta distribution is broader with higher yields at larger polar angles β. The differences in the C and Ta distributions originate from the different processes leading to sputtering. The peak in the C (and Ti) distributions is created by sputtering in (more or less) one binary collision [25, 26]. Similar differences in the angular distributions of Nb and B in the incident plane due to ion bombardment of NbB_2 have been observed experimentally [25] and by computer simulation [25]. Both angular distributions of C or Ta in the incident plane are nearly independent of the assumed stoichiometry: for initial conditions $Ta_{0.5}C_{0.5}$, "equilibrium conditions" $Ta_{0.78}C_{0.22}$, or for the pure element C or Ta. This is demonstrated in Fig. 18.

Whereas in the preceding Figs. 17 and 18 the angular distributions only in the incident plane are shown, the next Figs. 19 and 20 show complete angular distributions in the form of contour line plots. The lines connect points of equal intensities per solid angle and they are plotted versus the polar angle β, and the azimuthal angle φ. The angular resolution is 3°, so that a grid of 1800 points are used to produce the contour plot. The step between adjacent contour lines is given by c in arbitrary units (dependent on the number of incident particles).

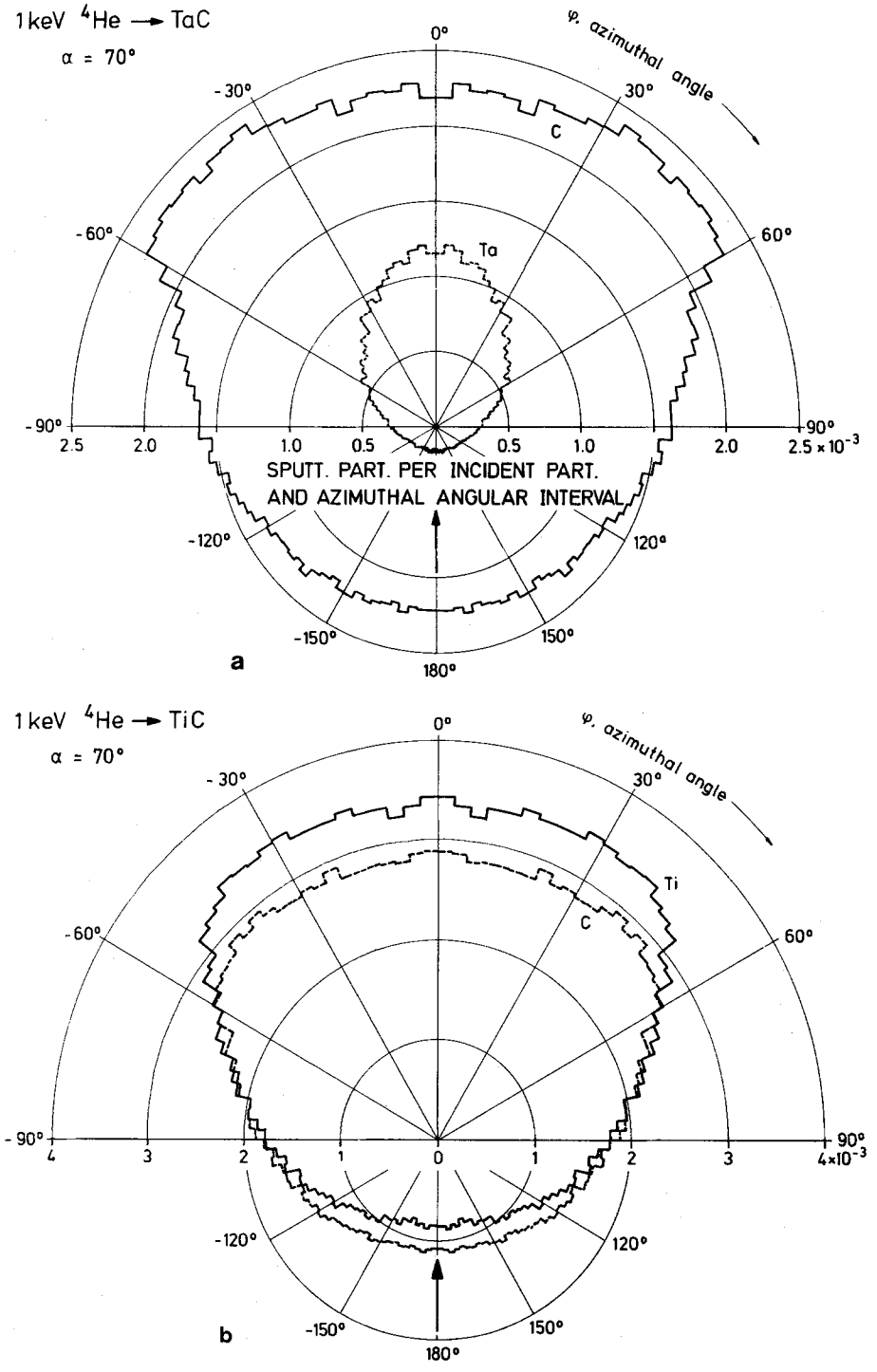

Fig. 16a and b. Azimuthal angular distributions (integrated over all polar angles) of sputtered atoms for 1 keV ^{4}He bombardment of TaC (a) and TiC (b) at an incident angle, $\alpha = 70°$

The complete angular distributions of the two constituents of the target can be very different, as shown in Fig. 19a for the bombardment of WC by 1 keV ^{4}He at an incident angle $\alpha = 70°$. The high intensity ridge seen in the C distribution is not visible in the W distribution. As demonstrated earlier [2], this ridge is due to PKA's. For higher incident energies such a ridge also appears in the W distribution. The maximum intensity appears always near the incident plane ($\varphi = 0$). For W the highest intensity is found at medium polar angles ($\beta \approx 45°$). (The structure near $\beta \approx 0°$ originates from bad statistics and should be ignored.)

For TiC and the same bombarding conditions as for WC, the distributions for C and Ti look very similar

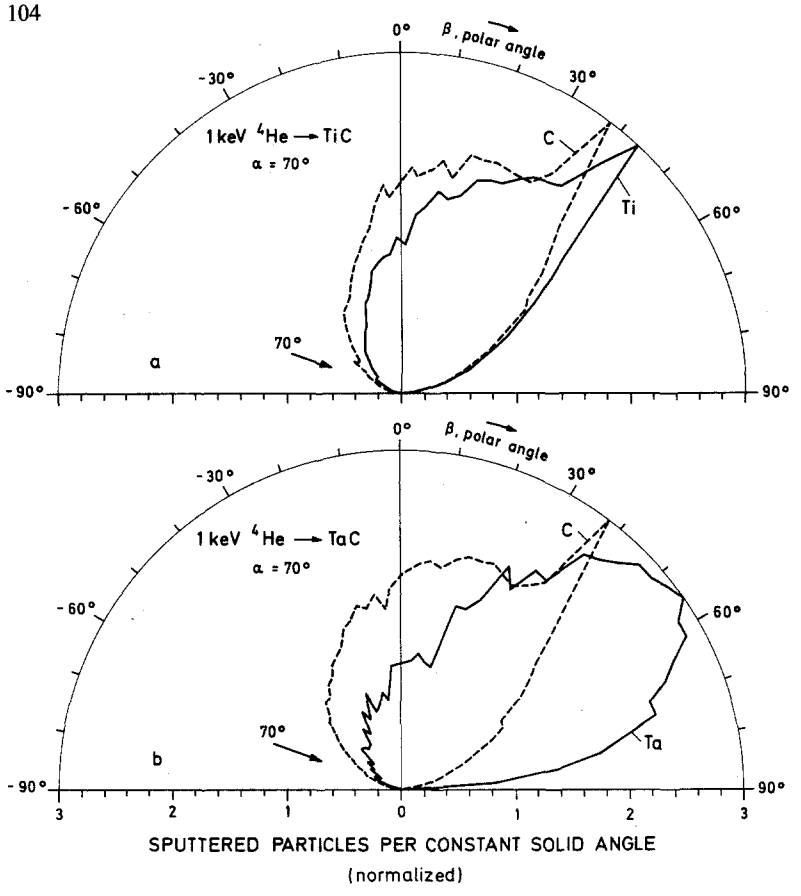

Fig. 17a and b. Polar angle distributions of sputtered particles in the incident plane (azimuthal angular range $0° < |\varphi| < 15°$ and $165° < |\varphi| < 180°$) for 1 keV ^{4}He bombardment at an incident angle, $\alpha = 70°$: (a) TiC, (b) TaC

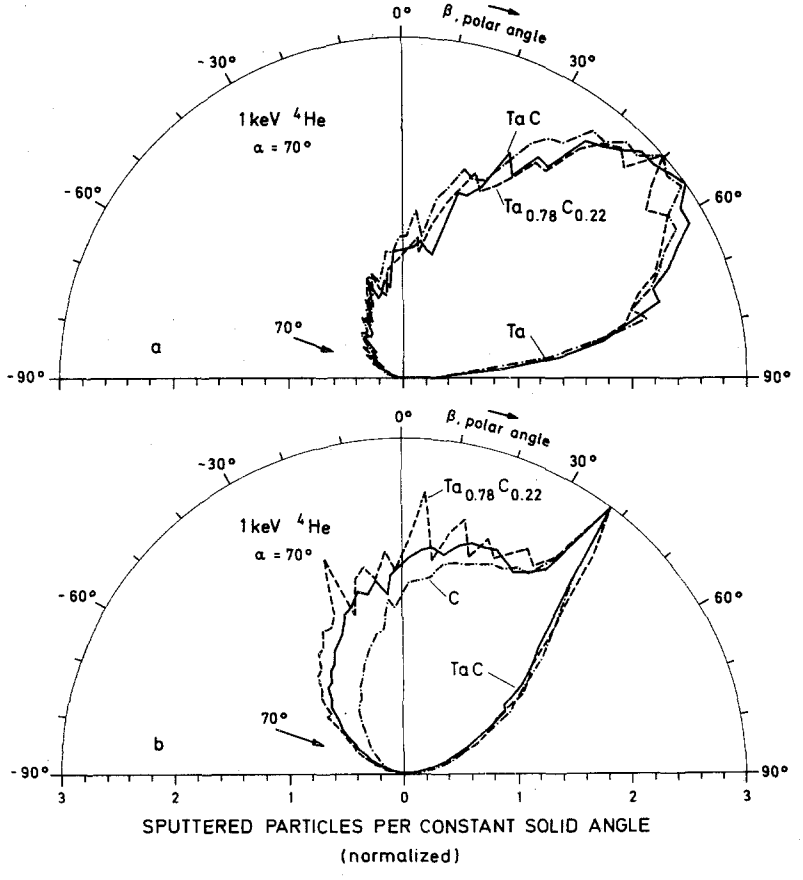

Fig. 18a and b. Polar angle distributions of sputtered particles in the incident plane (azimuthal angular range $0 < |\varphi| < 15°$ and $165° < |\varphi| < 180°$) for 1 keV ^{4}He bombardment of TaC (initial conditions), $Ta_{0.78}C_{0.22}$ (stationary conditions: stoichiometric sputtering) and Ta and C for comparison. Incident angle, $\alpha = 70°$. (a) Sputtered Ta atoms, (b) sputtered C atoms

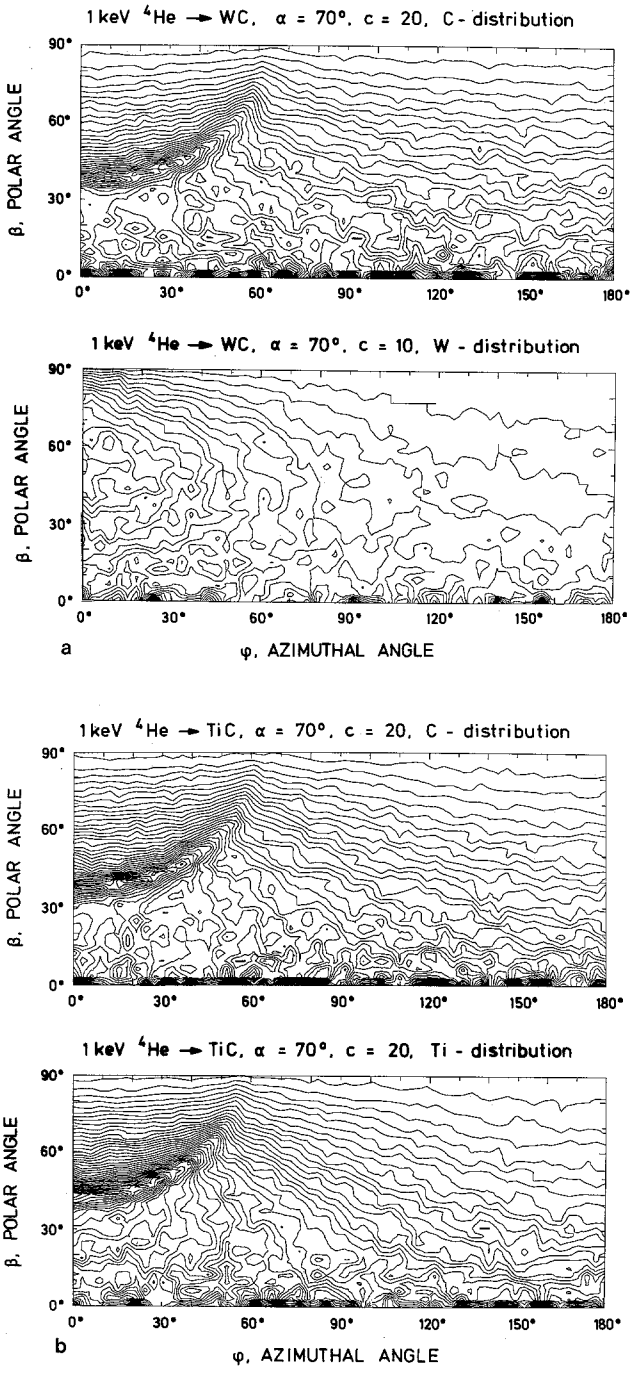

Fig. 19a and b. Complete angular distributions as contour plots (lines of equal intensity per solid angle). 1 keV ^{4}He bombardment at an incident angle, $\alpha = 70°$. (a) TaC, (b) TiC

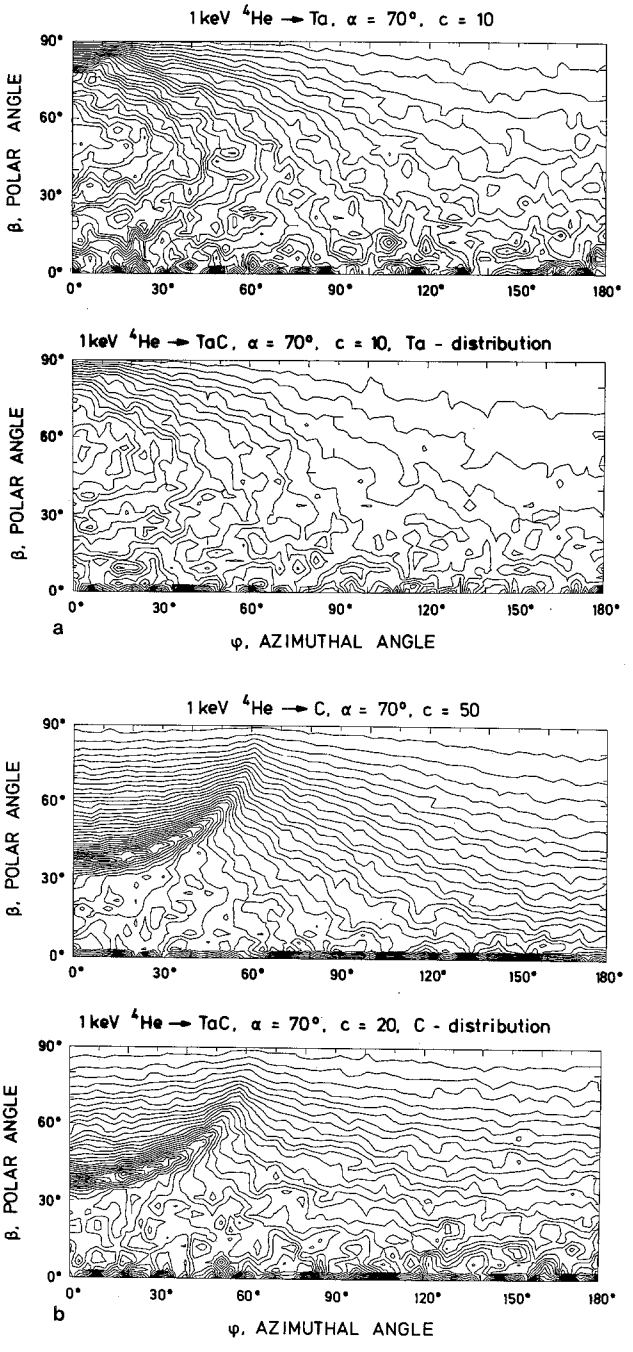

Fig. 20a and b. Complete angular distributions as contour plots (lines of equal intensity per solid angle). 1 keV ^{4}He bombardment at an incident angle, $\alpha = 70°$. (a) sputtered Ta atoms from a TaC and a Ta target; (b) sputtered C atoms from a TaC and a C target

(Fig. 19b). The only difference is that the high intensity ridge in the Ti distribution is shifted to larger polar angles and restricted to a smaller azimuthal angular range in comparison to the C distribution. This behaviour is explained by sputtering in one binary collision taking the planar surface potential into account [25, 26].

Figure 20 makes it clear that the complete angular distributions are not or only weakly dependent on the matrix. The Ta distributions from the bombardment of TaC and Ta by 1 keV ^{4}He at an incident angle $\alpha = 70°$ display hardly any difference. The same is true for the C distributions. This fact is still valid for "stoichiometric sputtering simulated by a changed bulk composition"

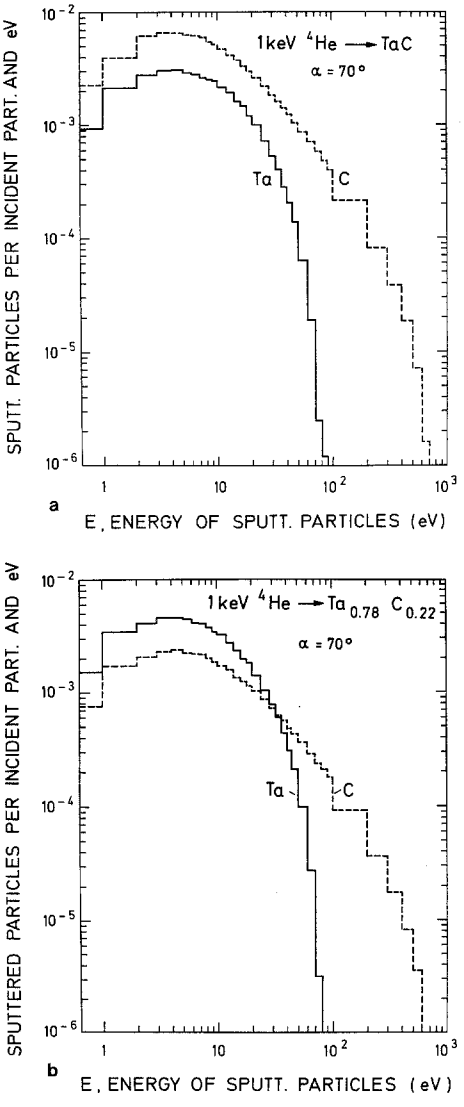

Fig. 21 a and b. Energy distributions of sputtered Ta and C atoms (integrated over all emission angles) for 1 keV ^{4}He at an incident angle, $\alpha = 70°$, bombarding. (a) TaC (initial conditions); (b) $Ta_{0.78}C_{0.22}$ (stationary conditions)

and even for a dynamic calculation [18]. For targets with different surface binding energies for both components, however, different angular distributions may result, as has been shown for boron sputtering from a variety of borides [19].

2.6. *Energy Distributions*

From the binary collision model it is expected, that the energy distributions of the two species of a compound are different at least, if the masses of the species differ. This can be observed in Fig. 21 a, where the Ta and C energy distributions (integrated over all emission angles) for the bombardment of TaC by 1 keV ^{4}He at an incident angle $\alpha = 70°$ are shown. Both energy

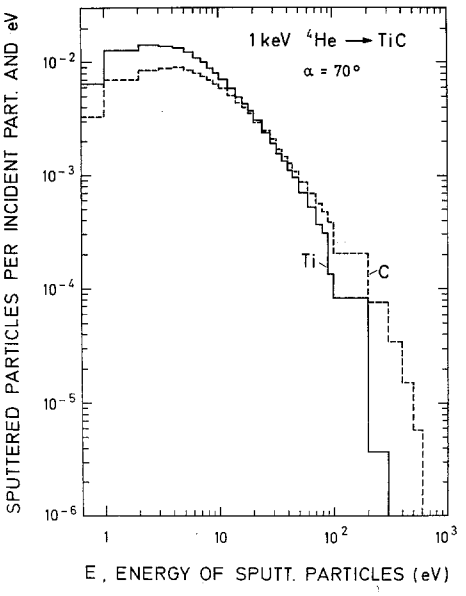

Fig. 22. Energy distributions of sputtered Ti and C atoms (integrated over all emission angles) for 1 keV ^{4}He bombardment of TiC at an incident angle, $\alpha = 70°$

distributions are very similar in shape at low energies. However, one finds more sputtered C atoms at higher energies. The entire high energy part of the spectrum is actually influenced by the high energy cut-off values, i.e. the maximum transferable energies to Ta or C atoms. The cut-off energy is 85 eV for Ta and 750 eV for C; in both cases the maximum is at 4 eV in good agreement with about 1/2 ΔH_s.

For bombardment at "equilibrium" with a bulk composition, $Ta_{0.78}C_{0.22}$, and the same incident conditions as above, the two distributions are shifted in such a way, that the C distribution has a lower intensity at low energies to account for stoichiometric sputtering (Fig. 21 b). A comparison of these distributions with those for initial conditions (TaC) show only very small differences in shape, but some differences in absolute intensities.

The last example, Fig. 22, shows the C and Ti distributions for the bombardment of TiC and for the same incident conditions as above. In this case the preferential sputtering is small (see also Sect. 2.2). Because the masses of both kinds of atoms are closer, the distributions differ less than for TaC. Furthermore the position of the maxima of both distributions clearly mirror the fact that the surface binding energy of C is larger than that of Ti, as the maximum is expected at 1/2 ΔH_s in the cascade theory [1].

Energy distribution in specific directions will exhibit a second maximum in forward directions ($\varphi < 90°$) as long as the complete angular distributions show a ridge created by PKA's. This effect has already been demonstrated in [2].

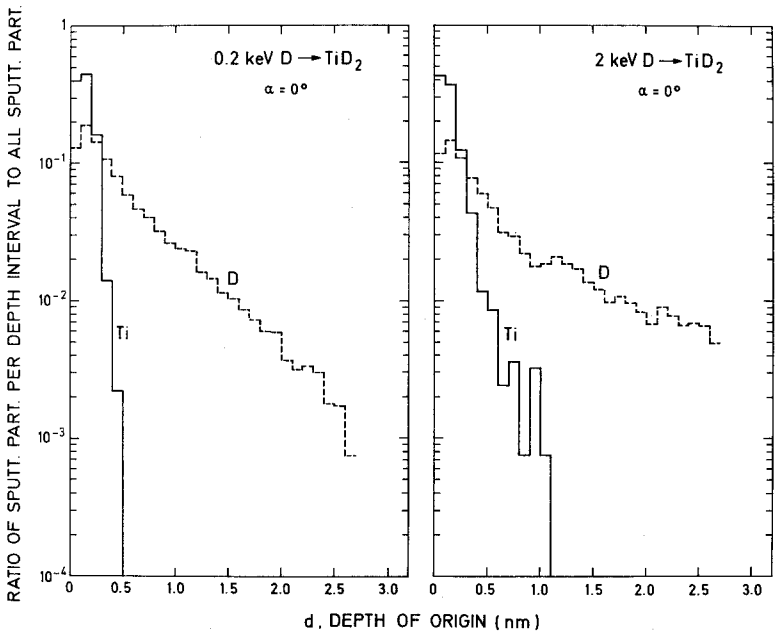

Fig. 23. Escape depth of sputtered particles: Relative number of sputtered particles versus their depth of origin (the first layer is at position $d=0$). TiD_2 is bombarded with 0.2 and 2 keV D at normal incidence

2.7. Depth of Origin of Sputtered Particles

It has been shown in [2] that the sputtered particles escape mainly from the first two layers. This is still true for targets if one component has not too low a mass. The situation changes somewhat for a target like TiD_2. This target is well suited to be studied by the static program used here, because Ti forms this stoichiometric deuteride at room temperature by continuous bombardment with D to depths, which are much larger than the range of the incident hydrogen [27]. That means there will be no concentration change in the target due to the bombardment. About 50% of the sputtered D escapes from the first two layers, the rest originates from many layers (Fig. 23). The contribution from deeper layers increases with increasing energy. Similar results but with poorer statistics have been given in [28].

3. Conclusions

This paper has demonstrated that the sputtering TRIM can also be applied to composite targets. It allows to calculate total and partial sputtering yields for a virgin target as well as approximately for stationary conditions. Computed surface concentrations at "equilibrium" seem to be in reasonable agreement with experimental data, exhibiting a stronger dependence on the incident energy than on the incident angle. Furthermore it is shown that the angular and energy distributions for a specific element depend only weakly on the target composition. Sputtering of isotope mixtures will lead to an enrichment of one isotope at the surface for someion target combinations and incident energies. The contributions of different processes are discussed for some examples. A comparison of experimental data and calculated results show that for the examples investigated collisional effects are sufficient to describe the experimental data.

Many other topics as the sputtering of alloys [18] or the ion desorption of adsorbed atoms have not been reported. Results will be published in forthcoming papers.

References

1. *Sputtering by Particle Bombardment* I, ed. by R. Behrisch, Topics Appl. Phys. **47** (Springer Berlin, Heidelberg 1981)
2. J.P. Biersack, W. Eckstein: Appl. Phys. **34**, 73 (1984)
3. M.L. Roush, T.D. Andreadis, O.F. Goktepe: Radiat. Eff. **55**, 119 (1981)
4. W. Möller, W. Eckstein: NIM B**2**, 814 (1984)
5. G. Betz, G.K. Wehner: In *Sputtering by Particle Bombardment* II, ed. by R. Behrisch, Topics Appl. Phys. **52** (Springer, Berlin, Heidelberg 1983) p. 11
6. H.H. Andersen: In *Ion Implantation and Beam Processing*, ed. by J.S. Williams, J.M. Poate (Academic, Sydney 1984) p. 128
7. P. Sigmund: J. Vac. Sci. Technol. **17**, 396 (1980)
8. P. Sigmund, A. Oliva, G. Falcone: Nucl. Instrum. Methods **194**, 541 (1982)
9. G. Falcone, A. Oliva: Appl. Phys. A**33**, 175 (1984)
10. *Secondary Ion Mass Spectrometry* SIMS II–IV, ed. by A. Benninghoven et al., Springer Ser. Chem. Phys. **9**, **19**, **36** (Springer, Berlin, Heidelberg 1979, 1982, 1984)
11. E. Hechtl, J. Bohdansky, J. Roth, J. Nucl. Mat. **103**, **104**, 333 (1981)
12. M. Kaminsky, R. Nielsen: Thin Solid Films **83**, 107 (1981)

13. W. Möller, W. Eckstein: NIM B**2** (in press)
14. E. Taglauer, W. Heiland: Proc. Symp. on Sputtering, ed. by P. Varga, G. Betz, F.P. Viehböck, Vienna (1980) p. 423
15. P. Varga, E. Taglauer: J. Nucl. Mat. **111**, **112**, 726 (1982)
16. R. Hultgren, R.L. Orr, P.D. Andersen, K.K. Kelly: *Selected Values for the Thermodynamic Properties of Metals and Alloys* (Wiley, New York 1963)
17. E. Taglauer: Private communication
18. W. Eckstein, W. Möller: NIM B**2** (1985) (in press)
19. J. Roth, J. Bohdansky, A.P. Martinelli: Radiat. Eff. **48**, 213 (1980)
20. M. Kaminsky, R. Nielsen, P. Zschack: J. Vac. Sci. Technol. **20**, 1304 (1982)
21. J.P. Biersack: Fusion Technol. **6**, 475 (1984)
22. R.R. Olson, M.E. King, G.K. Wehner: J. Appl. Phys. **50**, 3677 (1979)
23. G.K. Wehner, R.R. Olson, M.E. King: Proc. 7th Intern. Vac. Congr. and 3rd Intern. Conf. Solid Surfaces, Vienna (1977) p. 1461
24. J. Roth: Private communication
25. J. Roth, J. Bohdansky, W. Eckstein: Nucl. Instrum. Methods **128**, 751 (1983)
26. W. Eckstein: IPP-Report 9/41 (1983)
27. J. Roth, W. Eckstein, J. Bohdansky: Radiat. Eff. **48**, 231 (1980)
28. O.S. Oen, M.T. Robinson: J. Nucl. Mat. **76**, **77**, 370 (1978)